Robotica (2003) volume 21, pp. 59–69. © 2003 Cambridge University Press
DOI: 10.1017/S0263574702004319 Printed in the United Kingdom

Path planning by fractional differentiation

A. Oustaloup, B. Orsoni, P. Melchior and H. Linarès

Laboratoire d'Automatique et de Productique (LAP - UMR 5131 CNRS - Université Bordeaux 1 - ENSEIRB), 351 cours de la Libération, F 33405 Talence cedex (France). E-mail: melchior@lap.u-bordeaux.fr

(Received in Final Form: December 6, 2001)

SUMMARY

In path planning design, potential fields can introduce force constraints to ensure curvature continuity of trajectories and thus facilitate path-tracking design. The parametric thrift of fractional potentials permits smooth variations of the potential in function of the distance to obstacles without requiring design of geometric charge distribution. In the approach we use, the fractional order of differentiation is the risk coefficient associated to obstacles. A convex danger map towards a target and a convex geodesic distance map are defined. Real-time computation can also lead to the shortest minimum danger trajectory, or to the least dangerous of minimum length trajectories.

KEYWORDS: Mobile robots; Path planning; Potential field; Fractional differentiation; Risk coefficient.

1. INTRODUCTION

Path planning design is the elaboration of a strategy to define a trajectory which will reach a target avoiding obstacles.[1]

For fixed polygonal obstacles, the connectivity of the robot s free space can be captured in a network of nodes and arcs, the *roadmap*.[2] The nodes are the possible states of the robot, and the arcs are the possible transitions between nodes. A variety of roadmap types are available (visibility graph,[3] retraction approach,[4] freeway method,[5] silhouette method[6]) using a variety of development graph algorithms (depth-first, breast-first, A*[7,8] sweepline[9]). However, most of these algorithms are intractable; finding the optimal path to an unknown node in a weighted graph, is a NP-complete problem.[10]

The evaluation function can consider the maximum permitted speed towards an obstacle considering the shortest distance to it.[11] The real heading of the robot in relation to the obstacle is not considered. Only one heading is considered: frontal collision. Including discrete values for heading and speed would generate too many nodes and arcs. So, useable roadmap methods only provide geometric trajectories, and can be therefore inappropriate for time-optimal problems within path tracking.[12] The retraction approach, using Voronoï diagrams, provides maximum-security trajectories, but with angular points on cell intersections and thus jumpy steering and acceleration. Visibility graphs provide minimum length trajectories including angular points and contact with obstacles. Other global methods also lead to optimal trajectories according to a predefined criterion.[2]

To avoid complex computation, local methods can be used. The target position can be an omnidirectional light source emitting rays, which are diffracted on the edges of opaque impassable obstacles.[13] The robot follows the path towards the source of the ray. Potential field methods for path planning are often an alternative to graph searching techniques.[2,14] They introduce force constraints for practical speed control. The potential field concept considers the robot as a charged particle moving through repulsion potentials of obstacles, and attraction potentials of the target.[2] The combined potential values give a danger level at each point of the environment.[1,15] The potential gradient gives the norm and direction of the force field. In most cases the force norm is not used. The force direction provides the most appropriate heading for the robot to take. As the trajectory depends only on the local environment of the robot, it can be computed in real time. The smoothness of the curve obtained with potential-field methods, makes practical steering and speed control possible. However, the robot may not find a possible way through a narrow path. The robot may also be trapped in local minima as the algorithm always indicates the deepest point of potential cups. To avoid the local minima problem, superquadric potential fields have been defined.[1,14] However, only one obstacle can be considered at a time, and some particular initial and final positions can necessitate a re-calculation of the superquadric potential. This limits the application of this method and does not solve the narrow path problem.

Artificial potentials can be combined with heuristically guided searching techniques: a coulombian potential and A* algorithm can then be used.[16] Certainty grids can also generate potential fields to ease navigation.[17] A heuristic wall-following procedure can be applied here to avoid potential traps.[11] For the potential definition, the discrete distance considered may not correspond to a euclidean distance. The distance can be successively calculated along the frontiers of the Voronoï diagram, then extended from the skeleton to the whole free space.[18,19] The potential $1/d$, where d is the modified distance, provides valleys for the robot to follow.

The concept of danger for a trajectory comes from military requirements. For missiles, planning a trajectory through a map divided into quadrilaterals, can be used to escape from radar control.[20] A trajectory through enemy lines can be calculated by introducing a risk factor into the search criterion.[21]

This danger concept, which smoothly modifies the trajectory, is therefore of interest in trajectory planning for mobile robots. In the approach we use, the fractional order of differentiation is used as a risk coefficient for each obstacle, and determines the potential map created by the various obstacles.

The coulombian potential field generated by a punctual charge is the work (order one integration) done by the coulombian electric field. The coulombian potential of a uniformly charged infinite segment is obtained by summing over all infinitesimal segments (further integration). We define here a normalized fractional potential field with gradual passage between these two coulombian potentials. The fractional order of integration provides smooth and gradual modifications of potentials, without requiring geometric design of charge distribution.[22,23] Fractional potentials[24,25] can be numerically computed using Grünwald's definition.[24,26–29]

This paper is organized as follows: In Section 2, definitions about coulombian potential fields are given. Section 3 gives the definition of the fractional derivative. In Section 4, the *fractional potential map* is defined. Its normalization is presented in Section 5. In Section 6, the fractional-potential monotony and convexity are studied. In Section 7, the *fractional map* and the *fractional road* are defined. Finally, two global methods, using fractional potential maps, are presented in Section 8. These methods provide both minimum length and least dangerous trajectories.

The path planning methods we describe are in a 2D environment (operational space) for convenient presentation and illustration. However, the fractional potential methods can easily be applied to multidimensional environments (joint space).

2. COULOMBIAN POTENTIAL FIELD

2.1. Case of a punctual charge

The coulombian electric field $\mathbf{E}(\mathbf{r})$, generated in vacuum by a punctual charge, has a spherical symmetry. This electric field is thus radial, its norm only depending on the distance to the charge, and its forward or reverse direction is given by the polarity of the charge:

$$\mathbf{E}(\mathbf{r})=\frac{q}{4\pi\varepsilon_0 r^2}\,\mathbf{e}_\mathbf{r}, \tag{1}$$

where ε_0 is vacuum permittivity, r the distance to charge q, and $\mathbf{e}_\mathbf{r}$ a radial unit vector pointing from the punctual charge towards the point under consideration (Figure 1).

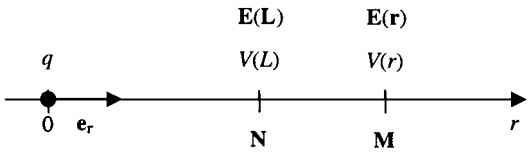

Fig. 1. Coulombian potential of a punctual charge.

The norm of the electric field is thus given by:

$$E(r)=\frac{q}{4\pi\varepsilon_0 r^2}. \tag{2}$$

The coulombian potential field generated by a charge distribution is, at each point of the free space, the potential energy per unit test charge. This potential is the work done by the electric field from the position under consideration to infinity (potential reference):

$$V(\mathbf{r})=\int_{\mathbf{r}}^{+\infty}\mathbf{E}(\mathbf{x})\,\mathrm{d}\mathbf{x}=-\int_{+\infty}^{\mathbf{r}}\mathbf{E}(\mathbf{x})\,\mathrm{d}\mathbf{x}. \tag{3}$$

Due to the spherical symmetry of the electric field (1), the vectorial integral (3) can be reduced to a scalar integral:

$$V(r)=-\int_{+\infty}^{r}E(x)\,\mathrm{d}x, \tag{4}$$

namely, by using (2):

$$V(r)=\frac{q}{4\pi\varepsilon_0 r}. \tag{5}$$

The potential difference $V_{\mathbf{MN}}$ between points **M** and **N** (potential reference at finite distance L) is then:

$$V_{\mathbf{MN}}=\frac{q}{4\pi\varepsilon_0}\left(\frac{1}{r}-\frac{1}{L}\right). \tag{6}$$

2.2. Case of a distributed charge

In the case of a linear charge Q, uniformly distributed on a segment of length X, the potential due to an infinitesimal segment of length $\mathrm{d}x$ and charge $\mathrm{d}q$ is given by:

$$\mathrm{d}V(x)=\frac{\mathrm{d}q}{4\pi\varepsilon_0 x}, \tag{7}$$

where $x=r+r_0$ (with $\mathrm{d}x=\mathrm{d}r$) is the length between the infinitesimal segment and the point under consideration as indicated in Figure 2.

The charge $\mathrm{d}q$ of the infinitesimal segment is:

$$\mathrm{d}q=\frac{Q}{X}\,\mathrm{d}x=\lambda\,\mathrm{d}x, \tag{8}$$

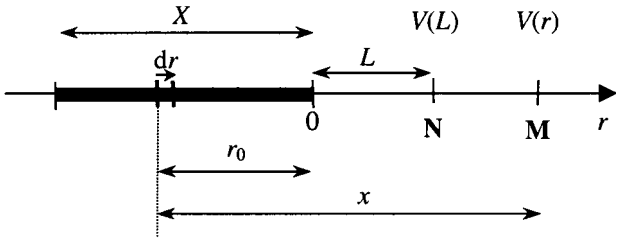

Fig. 2. Coulombian potential of a linearly distributed charge on a segment.

https://doi.org/10.1017/S0263574702004319 Published online by Cambridge University Press

λ denoting the uniform linear density of charge.

Combining Equations (7) and (8), $\mathrm{d}V(x)$ becomes:

$$\mathrm{d}V(x)=\frac{\lambda\,\mathrm{d}x}{4\pi\varepsilon_0 x}. \tag{9}$$

The total potential at distance r is obtained by summing over all infinitesimal segments. This requires integrating Equation (9) between $x=r+X$ and $x=r$:

$$V(r)=\int_{X+r}^{r}\mathrm{d}V(x)=\frac{\lambda}{4\pi\varepsilon_0}\int_{X+r}^{r}\frac{\mathrm{d}x}{x}, \tag{10}$$

or

$$V(r)=\frac{\lambda}{4\pi\varepsilon_0}\left[\ln(x)\right]_{X+r}^{r}, \tag{11}$$

or else

$$V(r)=\frac{\lambda}{4\pi\varepsilon_0}\ln\left(\frac{r}{r+X}\right). \tag{12}$$

The potential difference $\mathrm{V_{MN}}$ between the point under consideration **M** and the point **N** at finite distance L (potential reference) is then:

$$V_{\mathrm{MN}}=\frac{\lambda}{4\pi\varepsilon_0}\ln\left(\frac{r}{r+X}.\frac{L+X}{L}\right), \tag{13}$$

namely:

$$V_{\mathrm{MN}}=\frac{\lambda}{4\pi\varepsilon_0}\ln\left(\frac{r}{L}\right), \tag{14}$$

when $X\gg r, L$.

2.3. From coulombian potential to fractional potential

Modification of the distribution of charge Q could provide a gradual passage from (5) to (12), but this is not practical. We can achieve a gradual, even a smooth passage, by simply modifying an integration order.

A single integration provides the coulombian potential (5) from the electric field of a punctual charge. From the electric field of a punctual charge, two integrations provide the coulombian potential of a uniformly distributed charge along a straight-line segment (12). By considering more the operators than the integral bounds, the twice integrations, which provide (12), can be considered as the order two integral of the electric field generated by a punctual charge. Thus, from the electric field generated by a punctual charge, the passage from (5) to (12), can be achieved by a modification of the integration order from 1 to 2.

The fractional integration concept permits the gradual passage between the order 1 and order 2 integrals. Thus various fractional orders of integration, between 1 and 2, will provide various curves of potential between coulombian potentials of a punctual charge and a uniformly distributed charge along a straight-line segment. Obstacle influence, expressed as a risk coefficient, can thus be modified smoothly. So, fractional integration will control the potential shape, and there is no need to modify the charge distribution.

3. FRACTIONAL DERIVATIVE

3.1. Definition of fractional calculus

For a fractional derivative operator, output $s(t)$ is the n^{th} derivative of input $e(t)$:

$$s(t)=D^n e(t), \tag{15}$$

where $D=\mathrm{d}/\mathrm{d}t$ is the derivative operator, and n is no longer limited to being an integer: it can be also a fractional, real, imaginary or complex number.

When the real part of the fractional order is negative, it is in fact a fractional integral operator which is also defined by (15). So, we can refer to fractional derivative or fractional integral indifferently.

The fractional integral concept appeared in the 19^{th} century with Laplace, Liouville,[30] Abel[31] and Riemaunn.[32] Riemann's definition is:

$$D^{-n}f(t)=\frac{1}{\Gamma(n)}\int_{c}^{t}(t-\theta)^{n-1}f(\theta)\,\mathrm{d}\theta, \tag{16}$$

where c is the integral reference, $\Gamma(n)$ the gamma function, and n the fractional integration order. Unfortunately, for historical reasons, the word fractional is used in the literature. It is, however, understood as meaning any real, imaginary, or complex number.

3.2. Discrete form: Grünwald's definition

The first derivative of a function is defined by:

$$\mathrm{D}\,f(t)=\lim_{h\to 0}\frac{f(t)-f(t-h)}{h}. \tag{17}$$

Introducing the left finite difference $\Delta_h f(t)$, namely:

$$\Delta_h f(t)=f(t)-f(t-h), \tag{18}$$

or

$$\Delta_h f(t)=(1-q^{-1})f(t), \tag{19}$$

where q^{-1} is the delay operator, and h the finite sampling step, the effective computation of (17) is defined by:

$$\mathrm{D}\,f(t)=\frac{1-q^{-1}}{h}f(t). \tag{20}$$

If a function $f(x)$ is differentiable up to order n, expression (20) can be extended:

$$\mathrm{D}_h^n f(t)\approx\left(\frac{1-q^{-1}}{h}\right)^n f(t). \tag{21}$$

https://doi.org/10.1017/S0263574702004319 Published online by Cambridge University Press

Expression (21) can be used to define a fractional derivative by direct replacing n by a fractional order. It is one more time understood that n can be any real, imaginary, or complex number.

A series expansion of (21) leads to:

$$D^n f(t) \approx \frac{1}{h^n}\left(\sum_{k=0}^{\infty}(-1)^k a_k(n) q^{-k}\right) f(t), \tag{22}$$

where $a_k(n)$ are the binomial coefficients:

$$a_k(n) = \frac{\Gamma(n+1)}{\Gamma(k+1)\Gamma(n-k+1)}. \tag{23}$$

So, the fractional differentiation of a function will be computed using Grünwald's definition.[26]

$$D^n f(t) \approx \frac{1}{h^n}\sum_{k=0}^{\infty}(-1)^k a_k(n) f(t-kh). \tag{24}$$

This becomes the same as the Riemann-Liouville fractional integral when the sampling interval tends towards zero.[25] A negative real part for the fractional order of differentiation n is chosen for (24), so the fractional integral (16) can be computed.

Definition (24) shows that the fractional integral of a function at instant t takes into account the function values at all instants of its past: $f(t)$, $f(t-h)$, $f(t-2h)$, $f(t-3h)$ etc., which are samples of its history.

4. FRACTIONAL POTENTIAL DEFINITION

4.1. The fractional potential

A gradual passage between the potentials of a punctual charge and a uniformly distributed charge along a straight-line segment, can be obtained using fractional integral (16). We thus propose to define the fractional potential as the fractional integration of the electric field generated by a punctual charge with a fractional integration order n such that $\mathscr{R}e(n) \geq 1$:

$$V_n(r) = -D^{-n}E(r) = -\frac{q}{4\pi\varepsilon_0\Gamma(n)}\int_c^r \frac{(r-\theta)^{n-1}}{\theta^2}\,\mathrm{d}\theta. \tag{25}$$

As a distance r is always a positive number, the integral reference must be positive. Also, the electric field of a punctual charge is infinity when $r=0$. The integration reference c is thus chosen at the strictly positive, finite minimum-distance considered, L:

$$c = L. \tag{26}$$

4.2. Fractional integration of the electric when n = 1

When $n=1$, the fractlonal potential defined by expression (25) can be evaluated analytically:

$$V_1(r) = -\frac{q}{4\pi\varepsilon_0\Gamma(1)}\int_L^r \frac{(r-\theta)^0}{\theta^2}\,\mathrm{d}\theta, \tag{27}$$

or

$$V_1(r) = -\frac{q}{4\pi\varepsilon_0}\int_L^r \frac{1}{\theta^2}\,\mathrm{d}\theta, \tag{28}$$

namely:

$$V_1(r) = \frac{q}{4\pi\varepsilon_0}\left(\frac{1}{r} - \frac{1}{L}\right). \tag{29}$$

Expressions (6) and (29) are identical. The fractional potential obtained for $n=1$ is thus the coulombian potential of a punctual charge with a potential reference at a finite distance L.

4.3. Fractional integration of the electric field when n = 2

When $n=2$, the fractional potential defined by expression (25) can also be evaluated analytically:

$$V_2(r) = \frac{q}{4\pi\varepsilon_0\Gamma(2)}\int_L^r \frac{(r-\theta)^1}{\theta^2}\,\mathrm{d}\theta, \tag{30}$$

or:

$$V_2(r) = -\frac{q}{4\pi\varepsilon_0}\left[r\int_L^r \frac{1}{\theta^2}\,\mathrm{d}\theta - \int_L^r \frac{1}{\theta}\,\mathrm{d}\theta\right], \tag{31}$$

or else:

$$V_2(r) = \frac{q}{4\pi\varepsilon_0}\left[r\left[\frac{1}{\theta}\right]_L^r + [\ln(\theta)]_L^r\right], \tag{32}$$

or even:

$$V_2(r) = \frac{q}{4\pi\varepsilon_0}\left[1 - \frac{r}{L} + \ln\left(\frac{r}{L}\right)\right]. \tag{33}$$

For an integral reference such that $L \gg r$, expression (33) becomes:

$$V_2(r) = \frac{q}{4\pi\varepsilon_0}\ln\left(\frac{r}{L}\right), \tag{34}$$

which is similar to the coulombian potential of the uniformly distributed charge along a straight-line segment (14).

Such a reference, $L \gg r$, is not possible with Riemann's definition where $L < r$. However, this is possible when using Weyl's definition.[24–25]

As Equation (6) is the same as (29), and (14) the same as (34), a change in the charge distribution (from a punctual charge to a segment) can be considered as simply a modification of the fractional order of integration, n from 1 to 2.

https://doi.org/10.1017/S0263574702004319 Published online by Cambridge University Press

Rather than seeking to give an obstacle a charge distribution which depends on the risk the obstacle presents, we seek to give it simply an order of integration which takes the risk into account. The integration order, called the risk coefficient, suffices for determining the curvature of the potential created by the obstacle.

5. FRACTIONAL POTENTIAL NORMALIZATION

The fractional potential $V_n(r)$ is now normalized in [0 1]. $U_n(r)$ must be null (0% danger) at and greater than a finite distance considered as the maximum distance of influence $r_{\max}$. It must be made equal to unity (100% danger) at each obstacle to forbid collision. $U_n(r)$ is thus a percentage corresponding to the danger level:

$$U_n(r)=1-\frac{V_n(r)}{V_n(r_{\max})}. \tag{35}$$

Putting (25) into (35) provides the analytic expression of the normalized fractional potential $U_n(r)$:

$$U_n(r)=1-\frac{1}{K_n}\int_L^r \frac{(r-\theta)^{n-1}}{\theta^2}\,\mathrm{d}\theta. \tag{36}$$

where

$$K_n=\int_L^{r_{\max}} \frac{(r_{\max}-\theta)^{n-1}}{\theta^2}\,\mathrm{d}\theta. \tag{37}$$

So, the charge value, no longer affects the normalized fractional potential. Its shape is continuously controlled by the fractional integration order.

5.1. Computation using Grünwald's definition

In the particular case of a function $f(r)$, null when $r<L$:

$$\forall r>0,\ \exists k_0,\ \forall k>k_0,\ f(r-kh)=0; \tag{38}$$

k_0 is the integer part of $\dfrac{r-L}{h}$, namely

$$k_0=\left[\frac{r-L}{h}\right]. \tag{39}$$

Considering (26) and using (24), the fractional integral (25) can be computed with the following finite sum:

$$V_n(r)=\frac{qh^n}{4\pi\varepsilon_0}\sum_{k=0}^{k_0}\frac{a_k(n)}{(r-kh)^2}, \tag{40}$$

with k_0 given by (39).

The normalized fractional potential (35) then becomes:

$$U_n(r)\cong 1-\frac{1}{K_n}\sum_{k=0}^{k_0}\frac{a_k(n)}{(r-kh)^2}, \tag{41}$$

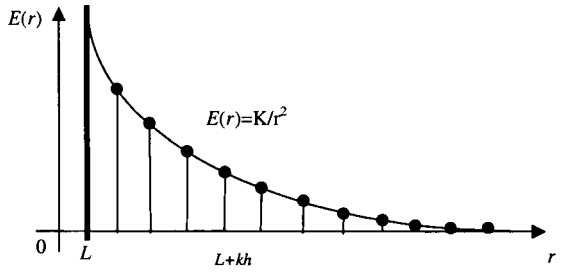

Fig. 3. Electric field $E(r)$ of a punctual charge at distance r from the finite minimum distance L.

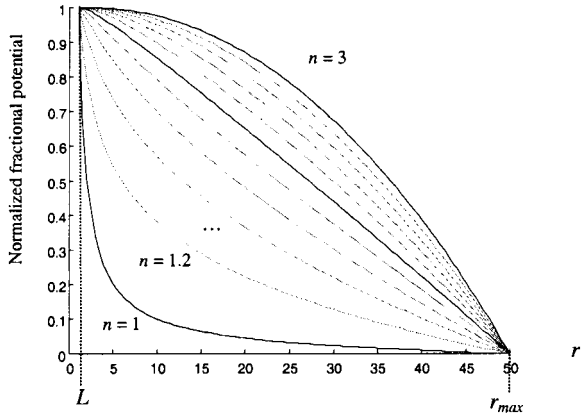

Fig. 4. Shapes of the fractional potential for various fractional integration orders: $n=[1;\ 1.2;\ 1.4;\ \ldots\ 2.8;\ 3]$, $L=1$, $r_{\max}=50$ and 10 samples by unit of distance ($n=1$: coulombian potential of a punctual charge).

where

$$K_n=\sum_{k=0}^{k_1}\frac{a_k(n)}{(r-kh)^2}, \tag{42}$$

with

$$k_1=\left[\frac{r_{\max}-L}{h}\right]. \tag{43}$$

5.2. The CRONE toolbox

The fractional potential is now computed using the function *dn* of the CRONE toolbox (MATLAB® language programs).[33] The computation of (40) through the *dn* function, is the discrete convolution product of the electric field, sampled at constant time intervals and considered null for $r<L$ (Figure 3) by the series of Newton binomial coefficients defined by (23).

The potential shapes obtained are shown on Figure 4. The more dangerous the obstacle, the greater the order of integration; also, the greater the influence area, the greater the potential at a given distance.

6. FRACTIONAL POTENTIAL MONOTONY AND CONVEXITY

Figure 5 shows a convexity transition of fractional potential shapes. The purpose of this section is to demonstrate

https://doi.org/10.1017/S0263574702004319 Published online by Cambridge University Press

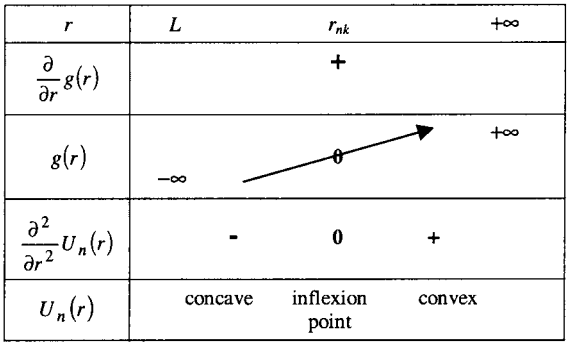

Fig. 5. Convexity of the fractional-potential for $1<n<2$.

analytically this phenomenon, and to prove the existence of an inflection point when the integration order n is between 1 and 2. The sign of the second derivative of $U_n(r)$ is therefore studied:

$$\frac{\partial^2}{\partial r^2}U_n(r)=-\frac{1}{K_n}\frac{\partial^2}{\partial r^2}\int_L^r\frac{(r-\theta)^{n-1}}{\theta^2}\,\mathrm{d}\theta, \tag{44}$$

where K_n is given by (37).

When $n>1$, integral and derivative operators can be permuted at least once:

$$\frac{\partial}{\partial r}U_n(r)=\frac{-(n-1)}{K_n}\int_L^r\frac{(r-\theta)^{n-2}}{\theta^2}\,\mathrm{d}\theta. \tag{45}$$

As $K_n>0$, $r>L$ and $n>1$, it can thus be deduced from (45) that $U_n(r)$ is an ever-decreasing function.

When $n>2$, integral and derivative operators can be permuted at least twice:

$$\frac{\partial^2}{\partial r^2}U_n(r)=-\frac{(n-2)(n-1)}{K_n}\int_L^r\frac{(r-\theta)^{n-3}}{\theta^2}\,\mathrm{d}\theta. \tag{46}$$

Thus, the fractional potential is concave.

When $1<n<2$, the permutation of operators is possible only once. To make the function to be integrated independent of r, the following change of variable is then used in expression (45):

$$rt=\theta; \tag{47}$$

thus:

$$\frac{\partial}{\partial r}U_n(r)=-\frac{(n-1)}{K_n}\int_{L/r}^1\frac{r^{n-2}(1-t)^{n-2}}{(rt)^2}\,r\,\mathrm{d}t, \tag{48}$$

or:

$$\frac{\partial}{\partial r}U_n(r)=\frac{-(n-1)}{K_n}[r^{n-3}f(r)], \tag{49}$$

where

$$f(r)=\int_{L/r}^1\frac{(1-t)^{n-2}}{t^2}\,\mathrm{d}t. \tag{50}$$

Differentiation of expression (49) gives:

$$\frac{\partial^2}{\partial r^2}U_n(r)=\frac{-(n-1)}{K_n}\left[r^{n-4}(n-3)f(r)+r^{n-3}\frac{\partial}{\partial r}f(r)\right] \tag{51}$$

with

$$\frac{\partial}{\partial r}f(r)=\frac{1}{L}\left(1-\frac{L}{r}\right)^{n-2}. \tag{52}$$

Lastly, combining (51) and (52) leads to:

$$\frac{K_n}{(n-1)r^{n-4}}\frac{\partial^2}{\partial r^2}U_n(r)=-(n-3)f(r)+\frac{r}{L}\left(1-\frac{L}{r}\right)^{n-2}. \tag{53}$$

As $n>0$, $K_n>0$ and $r>0$, the sign of $\frac{\partial^2}{\partial r^2}U_n(r)$ is that of function $g(r)$:

$$g(r)=-(n-3)f(r)-\frac{r}{L}\left(1-\frac{L}{r}\right)^{n-2}. \tag{54}$$

$g(r)$ is an ever-increasing function since:

$$\frac{\partial}{\partial r}g(r)=-\left(1-\frac{L}{r}\right)^{n-3}\frac{(n-2)}{L}>0. \tag{55}$$

The extreme values of $g(r)$ are thus reached at the extreme values of r:

$$g(L)=-\infty \quad \text{and} \quad g(+\infty)=+\infty. \tag{56}$$

To sum up, $U_n(r)$ is an ever-decreasing function $\forall n\geq 1$. Moreover,

- when $n=1$, the fractional potential is convex.
- when $1<n<2$, a convexity transition occurs according to Figure 5.
- when $n\geq 2$, the fractional potential is concave.

When $1<n<2$, the existence of the inflexion point depends on the $r_{\max}$ value If $r_{\max}<r_{nk}$, there is no inflexion point and the normalized fractional potential is concave whatever the value of the distance considered.

7. FRACTIONAL MAP AND FRACTIONAL ROAD

7.1. Risk coefficient

A refinement in path planning design is to establish a trajectory which differentiates the obstacles by considering

https://doi.org/10.1017/S0263574702004319 Published online by Cambridge University Press

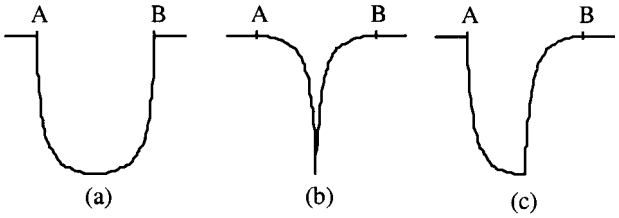

Fig. 6. Shapes of fractional-potential valleys between edges A and B of two obstacles: a) Wide valley allows passage close to either low-danger obstacle; b) Narrow valley restricts passage between two high-danger obstacles; c) Medium valley keeps the path far from the high-danger obstacle while allowing it to pass close to the low-danger obstacle.

their respective dangers, using any criterion adopted by robotics researchers.

As the risks of the various obstacles in an environment differ considerably, the trajectory can pass close to low-risk obstacles but must pass farther away from high-risk obstacles.

A fractional order of integration can modify smoothly the fractional potential influence without requiring, modification of the charge distribution. This fractional order can thus be used as the *risk coefficient* of obstacles. It thus modifies the curvature of the potential generated by the obstacles.

The fractional potential field map, called *fractional map*, must indicate a danger level for each point of the free space (Figure 6).

7.2. Distance map

To avoid area integrations the calculation of the potential field needs only depend on the nearest point of each obstacle.[2,34] The fractional-potential map can thus be deduced from the distance map using (36). The distance map from obstacles is thus computed first. A discrete geometry sequential algorithm is used here to optimize the processing time.[35] The distance map is determined by scanning the image of the environment from left to right and top to bottom in direct-video scan, using a *forward mask*, and then from right to left and from bottom to top by a *reverse mask*. The weightings of these masks are chosen to obtain a distance of *chanfrein*.[35] In discrete geometry, this distance minimizes the maximum error compared to a euclidean distance (Figures 7, 8 and 9).

The distance map is first initialized at $+\infty$ for each point in the free-space, and at zero within obstacles. A video-scan provides for each point a new value for $x_{i,j}$:

$$x_{i,j} \leftarrow \min \begin{bmatrix} x_{i-1,j-1}+4 & x_{i-1,j}+3 & x_{i-1,j+1}+4 \\ x_{i,j-1}+3 & x_{i,j} & \end{bmatrix}, \quad (57)$$

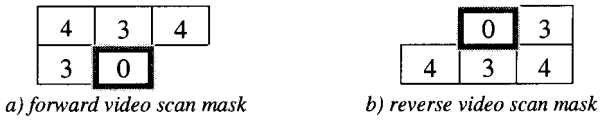

Fig. 7. Video-scan masks used in the sequential algorithm to compute the map of distances between nearest obstacle and point considered; highlighted box indicates the application point.

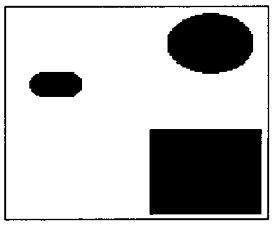

Fig. 8. Robot environment (white: free; black: obstacles).

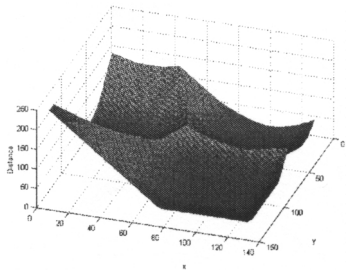

Fig. 9. 3D chanfrein distance map computed with a sequential algorithm; height is distance from nearest obstacle.

where i and j are respectively the line and column indices of the point under consideration.

The new value for each point affects the values of all points processed after. Once the last point of the direct-video scan has been processed, the inverse video-scan begins also providing a new value for $x_{i,j}$ for each point:

$$x_{i,j} \leftarrow \min \begin{bmatrix} & x_{i,j} & x_{i,j+1}+3 \\ x_{i+1,j-1}+4 & x_{i+1,j}+3 & x_{i+1,j+1}+4 \end{bmatrix}. \quad (58)$$

The distance map is determined using just two video-scans and thus only two computations per point.

7.3. Fractional potential map

Using (36), the distance map for each obstacle can now be converted into a potential map. The highest potential for each point is taken from these maps, providing the global fractional map (Figure 10). Discontinuity of force field directions is encountered, but local maximum values of potentials are avoided. The sum of the potential maps could be used to provide the global fractional potential map, but danger levels would not be normalized and so no longer correspond to a percentage.

7.4. Fractional road

The operator chooses a threshold danger level. The horizontal cross-section at this threshold on the fractional-potential map (Figures 11 and 12) provides a set of equipotentials. This set defines the edges of the *fractional road* that the robot must use. The fractional road thus imposes respect of a security distance around the obstacles. This distance depends on the danger level of obstacles: the greater the danger, the greater the security distance. This

https://doi.org/10.1017/S0263574702004319 Published online by Cambridge University Press

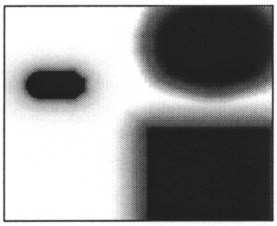

a) 2D fractional-potential map; grey scale indicates danger level

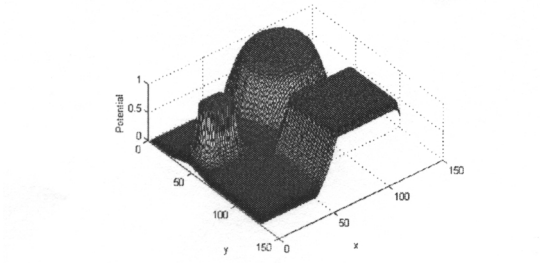

b) 3D fractional-potential map; height is danger level

Fig. 10. Example of a fractional-potential map; risk coefficients are 1.2 for the square, 1.5 for the small rounded rectangle and 2.5 for the oval obstacle; maximum distance of influence is $r_{max}=20$, minimum distance of evaluation is $r_{min}=1$.

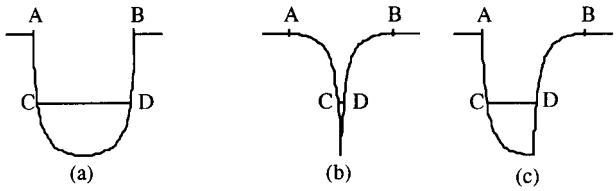

Fig. 11. Between edges A and B of two obstacles, the horizontal cross-section of the fractional-potential valley defines the fractional road where C-D is the width of the road: a) Wide road allows passage close to either low-danger obstacle; b) Narrow road restricts passage between two high-danger obstacles; c) Medium road keeps the possible path far from the high-danger obstacle while allowing passage close to the low-danger obstacle.

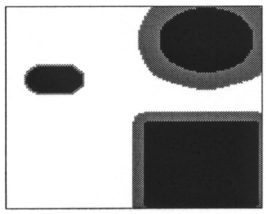

Fig. 12. Example of a fractional road for threshold danger level set at 50%; risk coefficients are fixed arbitrarily at 1.2 for the square, 1.5 for the small rounded rectangle and 2.5 for the oval obstacle (white: free space; grey: danger area; black: obstacles).

protects the robot against collisions but reduces the available space (Figure 12).

8. MINIMAL LENGTH OR MINIMAL DANGER TRAJECTORIES

8.1. Minimum length trajectories

The minimum distance trajectory is now obtained by gradient descent: successive steps, following the gradient of the geodesic distance map (Figures 13 and 14), provide the trajectory (Figure 15).

A parallel algorithm computes the geodesic map of distances from the target point: the values computed at iteration k are independent of the other values during the same iteration and only depend on the values of the previous iteration $(k-1)$.

First, the geodesic distances of the map are initialized at $+\infty$, except the target point which is initialized at 0. Second, the following parallel treatment is applied using a 3×3 chanfrein mask:[35]

$$x_{i,j}^{(k)} \leftarrow \min\left(\begin{bmatrix} x_{i-1,j-1}^{k-1} & x_{i-1,j}^{k-1} & x_{i,j+1}^{k-1} \\ x_{i,j-1}^{k-1} & x_{i,j}^{k-1} & x_{i,j+1}^{k-1} \\ x_{i+1,j-1}^{k-1} & x_{i+1,j}^{k-1} & x_{i+1,j+1}^{k-1} \end{bmatrix} + \begin{bmatrix} 4 & 3 & 4 \\ 3 & 0 & 3 \\ 4 & 3 & 4 \end{bmatrix} \right). \tag{59}$$

Finally, distance values on obstacles are re-initialized to $+\infty$:

$$\mathbf{X}^{(k)} \leftarrow \mathbf{X}^{(k)} + \mathbf{M}, \tag{60}$$

where $\mathbf{M}$ is a mask ($+\infty$ on obstacles; 0 on free space).

The procedure stops when X(k) is stationary:

$$\mathbf{X}^{(k)} = \mathbf{X}^{(k-1)}. \tag{61}$$

As the geodesic distance map is now available, the minimal length trajectory is thus computed from the start point to the target. For each point of the trajectory, the geodesic lengths

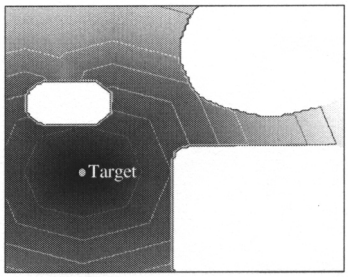

Fig. 13. 2D geodesic distance map; equipotentials give grey scale showing minimum distance available towards target; geodesic distances from points not on the road (white areas) are arbitrarily fixed at maximum.

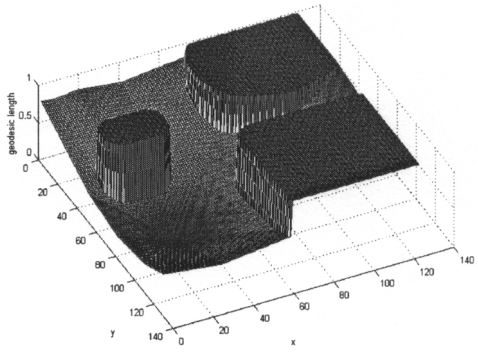

Fig. 14. 3D geodesic distance map; height gives minimum distance available towards target ($y=80$, $x=30$); height of points not on the road is arbitrarily fixed at maximum.

https://doi.org/10.1017/S0263574702004319 Published online by Cambridge University Press

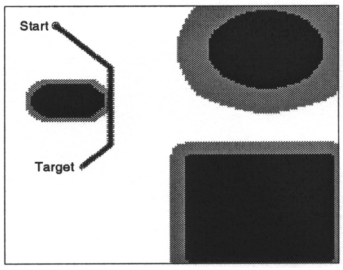

Fig. 15. Minimum length trajectory on the road from the start point to the target (white: free space; grey: dangerous area; black: obstacles).

to the target of the 8 neighbors are taken from the geodesic map. The lengths inferior to 3 (adjacent neighbors) or to 4 (diagonal neighbors) are selected. The minimum distance trajectory is not unique due to discrete evaluation. The fractional potential map is then used to select the least dangerous neighbor which becomes the next point of the trajectory. This procedure is iterated until the target is reached. The trajectory obtained is illustrated in Figure 15.

The least dangerous minimum length trajectory is obtained. The true euclidean distance is only approximated here, using the 3×3 chanfrein mask. Without obstacles, isodistance curves are octagonal polygons, which give a good approximation of true circles.[36] However a fast-marching algorithm[37] can be used to improve the precision of isodistance curves, and thus to design the true minimum length trajectory more precisely.

8.2. Minimum danger trajectories

The danger of a trajectory will be defined as the curvilinear integral of the potential (danger from the environment) on the trajectory. The danger map towards a target will also be defined, providing for each point of the free space, the minimum danger of the available trajectories reaching the target. This danger towards the target is also called *energy*.[36,38] But this term is not used here to avoid confusion with the real potential energy.

The minimum danger trajectory is also obtained by gradient descent: successive steps, following the gradient of the danger map towards the target (Figures 16 and 17), provide the trajectory (Figure 18).

Another parallel algorithm computes the danger map towards the target point.

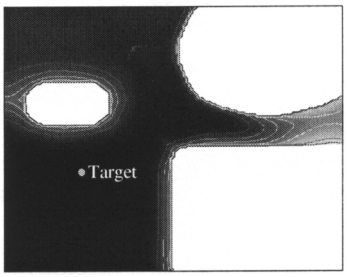

Fig. 16. 2D danger map towards the target; equipotentials give grey scale showing the minimum danger of the available trajectories; danger towards the target from points not on the road are fixed at maximum.

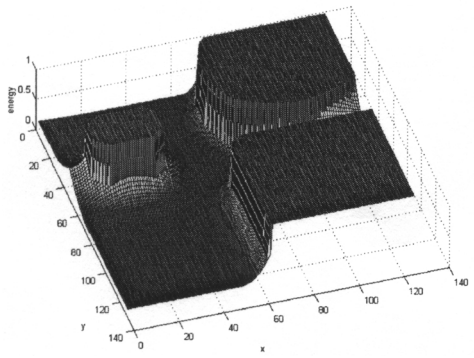

Fig. 17. 3D danger map towards the target ($y=80$, $x=30$); height gives the minimum danger of the available trajectories; height of points not on the road is arbitrarily fixed at maximum.

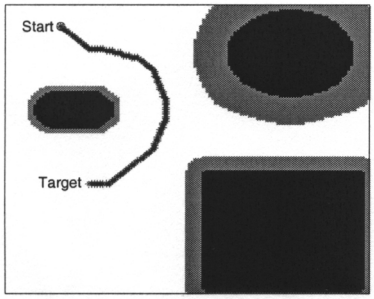

Fig. 18. Minimum danger trajectory on the road from the start point to the target (white: free space; grey: dangerous area; black: obstacles).

First, the danger map towards the target is initialized at $+\infty$, except the target point which is initialized at 0. Second, the following parallel treatment is applied:

$$x_{i,j}^{(k)}=\min\left(\begin{bmatrix} x_{i-1,j-1}^{k-1} & x_{i-1,j}^{k-1} & x_{i-1,j+1}^{k-1} \\ x_{i,j-1}^{k-1} & x_{i,j}^{k-1} & x_{i,j+1}^{k-1} \\ x_{i+1,j-1}^{k-1} & x_{i+1,j}^{k-1} & x_{i+1,j+1}^{k-1} \end{bmatrix} + \begin{bmatrix} p_{i-1,j-1} & p_{i-1,j} & p_{i-1,j+1} \\ p_{i,j-1} & 0 & p_{i,j+1} \\ p_{i+1,j-1} & p_{i+1,j} & p_{i+1,j+1} \end{bmatrix}\right) \tag{62}$$

where $p_{i,j}$ is the element at the i^{th} line and j^{th} column of the fractional potential map.

Finally, danger values on obstacles are re-initialized to $+\infty$:

$$\mathbf{X}^{(k)}\leftarrow\mathbf{X}^{(k)}+\mathbf{M}, \tag{63}$$

where $\mathbf{M}$ is a mask ($+\infty$ on obstacles; 0 on free space).

The procedure stops when $\mathrm{X}(k)$ is stationary:

$$\mathbf{X}^{(k)}=\mathbf{X}^{(k-1)}. \tag{64}$$

From the danger map towards the target now available, the minimal danger trajectory is thus computed from the start point to the target. For each point of the trajectory, the danger towards the target, of the 8 neighbors, are taken from the danger map towards the target. The next point of the trajectory is the least danger towards the target neighbor. If

https://doi.org/10.1017/S0263574702004319 Published online by Cambridge University Press

two neighbors have the same minimum danger, the geodesic distance map is used to select the nearest from the target.

The trajectory obtained is illustrated in Figure 18. The shortest of the least dangerous trajectories is retained. Curvatures obtained are not always smooth, but in this case they are smooth (Figure 18). Unlike the trajectory of retraction approach;[4] a minimum danger trajectory is not restricted to the minimum potential valley. The greater the trajectory length, the greater the number of potentials to be summed, so the minimum danger trajectory found is both smooth and short.

9. CONCLUSION

The fractional integral permits a gradual passage between two integer orders of integration, and thus between the coulombian potential shapes generated by a punctual charge and by a uniformly distributed charge along a straight-line segment. The fractional order is used as a *risk coefficient* to characterize the danger of obstacles. The parametric thrift of fractional integration is used here to smoothly modify the influence map of obstacles according to the danger the obstacles present, without requiring a modification of the charge distribution.

Thus, the fractional potential map gives a danger level for each point of the free space. Given a maximum admissible danger-level, the robot must be guided through the fractional road map. The security distance around obstacles depends on the risk coefficient associated to obstacles: the greater the danger, the greater the security distance. Although this reduces the road space, the robot is protected from collision.

Fractional potentials are not only used to determine danger areas, but also to compute optimal trajectories. The map of geodesic distances towards the target is convex and thus with only one global minimum: the target. A gradient descent, from any starting point can be computed in real-time. The fractional potential is used here to obtain the least dangerous minimum length trajectory. From the fractional potential, a danger map towards a target can be built. This danger map towards the target provides the minimum curvilinear integral of the fractional potential from the point under consideration to the target. This danger towards the target is also called *energy in image processing*. The danger map towards the target is thus also a convex map, with the target as the single global minimum. A gradient descent, whatever the starting point, computes in real-time the least dangerous trajectory.

Thus, in path planning design, the fractional potential easily determines the least dangerous of the minimum length trajectories, or the shortest of the least dangerous trajectories. Also, using a global method avoids minimumpotential traps.

A new fractional path-planning method using both length and energy now needs to be designed. The definitions of energy or danger towards the target can be improved.[36,38] A new convex map can also be designed using a weighting factor which considers both fractional potential and displacement. A heuristically guided technique, A* for example, would reduce computation time. Such an algorithm would also permit the inclusion of dynamic constraints (actuator band-pass, limited curvature radius, bending modes . . .).

The use of fractional potentials will provide an integrated method of path planning and tracking design. The method under construction,[39] aims at determining the time optimal trajectory with obstacles of any shape and considering actuator limitations. A procedure must be designed to fix non-arbitrarily both the risk coefficients and the threshold danger level, for a given environment.

References

1. R. Volpe and P. Khosla, "Manipulator control with superquadric artificial potential functions: theory and experiments", *IEEE Trans. on Systems, Man and Cybernetics* **20**, No. 6, 1423–1436 (1990).
2. J. C. Latombe, *Robot Motion Planning* (Kluwer Academic Publishers, fourth printing, 1996).
3. N. J. Nilsson, "A mobile automation: an application of artificial intelligence techniques", *1st International Joint Conference on Artificial Intelligence*, Washington D.C., USA (1969) pp. 509–520.
4. C. O'Dunlaing, M. Sharir and C. K. Yap, "Retraction: a new approach to motion planning", *15th ACM Symposium on the Theory of Computing*, Boston, USA (1983) pp. 207–220.
5. R. A. Brooks, "Solving the find-path problem by good representation of free space", *IEEE Trans. on Systems, Man and Cybernetics* **13**, No. 3, 190–197 (1983).
6. J. F. Canny, *The Complexity of Robot Motion Planning* (MIT Press, Cambridge, MA, USA, 1988).
7. N. J. Nilsson, *Problem-solving Methods in Artificial Intelligence* (McGraw-Hill, 1971).
8. H. Farreny, "Recherche heuristiquement ordonnée: généralisations compatibles avec la complétude et l'admissibilité", *Technique et Science Informatiques, RAIRO* **16**, No. 7, 925–953 (1997).
9. J. L. Bentley and T. A. Otttmann, "Algorithms for reporting and counting geometnc intersections", *IEEE Trans. on Computers*, No. 28, 643–647 (1979).
10. E. Koutsoupias, C. Papadimitnou and M. Yannakakis, "Searching a fixed graph", *International Colloquium on Automata, Languages and Programming*. Paderbom, Germany (July, 1996) pp. 280–289.
11. J. Borenstein and Y. Koren, "Real time obstacle avoidance for fast mobile robots", *IEEE Trans. on Systems, Man and Cybernetics* **19**, No. 5, 1179–1187 (1989).
12. W. Khalil and E. Dombre, *Modélisation, Identification et Commande des Robots* (Editions Hermès, Paris, 1999).
13. R. S. Alexander and N. C. Rowe, "Path planning by optimal-path-map construction for homogeneous-cost two-dimensional regions", *Proc. of IEEE International Conference on Robotics and Automation*, Cincinnati (May, 1990) pp. 1924–1929.
14. A. Pruski, *Robotique Mobile, Planification de Trajectoire* (Editions Hermès, Paris, 1996).
15. O. Khatib, "Real time obstacle avoidance for manipulator and mobile robot", *Int. J. Robotics Research* **5**, No. 1, 90–98 (1986).
16. B. H. Krogh and C. E. Thorpe, "Integrated path planning and dynamic steering control for autonomous vehicles", *Proc. IEEE International Conf. on Robotics and Automation*, San Francisco, USA (April, 1986) pp. 1664–1669.
17. N. Lefort-Piat, I. Collin et D. Meizel, "Planification des missions de robots mobiles référencés par rapport à l'environnement: tâche-robot et cartes locales", *Revue d'Intelligence Artificielle* **11**, No. 4, 489–516 (1997).
18. J. Barraquand, B. Langlois and J. C. Latombe, "Robot Motion Planning with Many Degrees of Freedom and Dynamic Constraints", *Robotics Research* (Eds. H. Miura and S.

https://doi.org/10.1017/S0263574702004319 Published online by Cambridge University Press

Arimoto) (MIT Press, Cambridge, MA, USA, 1990) pp. 435–444.
19. J. Barraquand and J. C. Latombe, "Robot motion planning: a distributed representation approach", *Int. J. Robotics Research* **10**, No. 6, 628–649 (1991).
20. T. R. MacMillan, C. E. Gerber, J. M. Sackett and P. D. Holden, "Knowledge based route planning", *Proc. of IEEE NAECON*, Dayton Convention Center (May, 1990) pp. 1001–1007.
21. P. L. Bergier, "Planification de missions et contre-mobilité: deux utilisations d'algorithmes de la robotique mobile", *Proc. Congrès EC2 "Les systèmes experts et leurs applications"*. Avignon, France (1991) pp. 101–108.
22. H. Linarès, "Modélisation d'environnement par dérivation non entière et commande robuste d'un robot mobile", *Thèse de doctorat de l'Université Bordeaux* I (29 Février, 1996).
23. A. Oustaloup, X. Moreau and H. Linarès, "The CRONE path planning", *Proc. 3rd ECPD International Conference on Advanced Robotics, Intelligent Automation and Active Systems*, Bremen, Germany (September, 1997) pp. 315–319.
24. K. S. Miller and B. Ross, *An Introduction to the Fractional Calculus and Fractional Differential Equations* (Wiley-Interscience Publications, 1993).
25. S. G. Samko, A. A. Kilbas and O. I. Marichev, *Fractional Integrals and Derivatives* (Gordon and Breach Science Publishers, 1993).
26. A. K. Grünwald, "Uber begrenzte Derivationen und deren Anwendung", *Z. Angew. Math. Phys*., No. 12, 441–480 (1867)
27. A. Oustaloup, *La Dérivation non entière: théorie, synthèse et applications* (Editions Hermès, Paris, 1994).
28. A. Oustaloup and H. Linarès, "The CRONE path planning", *Proc. IEEE-SMC/IMACS International Symposium on Signal Processing, Robotics and Neural Networks*, Lille France (1994) pp. 117–120.
29. A. Oustaloup and H. Linarès, "The CRONE path planning", *International IMACS Journal Mathematrics and Computers in Simulation*, No. 41, 209–217 (1996).
30. J. Liouville, "Mémoire sur quelques questions de géométrie et de mécanique et sur un nouveau genre pour résoudre ces questions", *J. Ecole Polytechnique*, No. 13, 1–69 (1832).
31. N. H. Abel, "Solution de quelques problèmes à l'aide d'intégrales définies", *Gesammelte Mathematische Werke* (Leibzig: Teubuer, , 1881) No. 1, pp. 11–17.
32. B. Riemann, "Versuch einer allgemeinen Auffassung der Integration und Differentiation", **In:** *Gesammelte Mathematische Werke und Wissenschaftlicher* (Leibzig: Teubner, 1876) pp. 331–344.
33. P. Melchior, P. Lanusse, F. Dancla and O. Cois, "Valorisation de l'approche non entière par le logiciel CRONE", *Proc. CETSIS-EEA'99*, Montpellier, France (1999) pp. 335–338.
34. Y. K. Hwang and N. Ahuja, "A potentiel field approch to path planning", *IEEE Trans. on Robotics and Automation* **8**, No. 1, 23–32 (1992).
35. J. M. Chassery and A. Montanvert, "Géometrie discrète en analyse d'images", **In:** *Traité des Nouvelles Technologies*. Editions Hermès, Paris (1991) Chapter 4, pp. 101–174.
36. L. D. Cohen and R. Kimmel, "Global Minimum for Active Contour Models: A Minimal Path Approach", *Int. J. Computer Vision* **24**, No. 1, 57–78 (1997).
37. J. A. Sethian, "A Fast Marching Level Set Method for Monotonically Advancing Fronts", *National Academy of Sciences* **93**, No. 4, 1591–1595 (1996).
38. F. Angella, O. Lavialle and P. Baylou, "A Deformable and Extensible Tree for Structure Recovery", *Proc. of IEEE Int. Conf. on Image Proc*., Chicago, USA (1998) No. 1, pp. 241–245.
39. B. Orsoni and P. Melchior, "Planification de trajectoire basée sur l'utilisation d'un potentiel non entier", *Proc. IEEE-CIFA '2000*, Lille, France (July, 2000) pp. 819–826.

https://doi.org/10.1017/S0263574702004319 Published online by Cambridge University Press